Eur. Phys. J. D **46**, 103–109 (2008)
DOI: 10.1140/epjd/e2007-00281-7

THE EUROPEAN PHYSICAL JOURNAL D

Diagnosis of negative hydrogen ions and rovibrational distribution of H_2 molecule in non-thermal plasmas

W.G. Wang[1], Y. Xu[1,2,a], X.F. Yang[1,2], A.M. Zhu[1,2], Z.W. Liu[1], and X. Liu[1]

[1] Laboratory of Plasma Physical Chemistry, P.O. Box 288, Dalian University of Technology, 116024 Dalian, P.R. China
[2] State Key Laboratory of Materials Modification by Laser, Ion and Electron Beams, Dalian University of Technology, 116024 Dalian, P.R. China

Received 14 February 2007 / Received in final form 7 July 2007
Published online 5 October 2007 –

Abstract. Rovibrational excited hydrogen molecule plays an important role for the production of H^- ions. The correlation between H^- ion density and rovibrational distribution of H_2 molecules has been investigated in dielectric barrier discharge hydrogen plasmas via optical emission spectrometry and molecular beam mass spectrometry. The relative vibrational distribution of molecular hydrogen in the electronic ground state has been determined by the best fitting to the Fulcher-α band emission lines. It is shown that the ratio of the $Q_{(0-0)}(1)$ to $Q_{(1-1)}(1)$ line is very suitable and simple for the diagnosis of vibrational temperature in the range of 1500 to 7500 K. At certain discharge conditions (ac 40 kHz, 14 kV), the vibrational temperature decreases from 3600 to 2400 K as the pressure increases from 100 to 200 Pa and the negative ions density near the ground electrode also decreases as the pressure increases. Both the hydrogen ions density and the vibrational temperature increase with the increasing of discharge voltage. It is found that the evolution of negative atomic hydrogen ions density greatly depends on the vibrational temperature.

PACS. 39.30.+w Spectroscopic techniques – 52.70.-m Plasma diagnostic techniques and instrumentation – 50. Physics of gases, plasmas, and electric discharges

1 Introduction

Hydrogen plasmas are widely used in the field of modern science and technology, especially material treatment: two intensely developed applications are surface cleaning or etching of compound semiconductors [1,2] and deposition of thin films [3] in pure hydrogen plasma or where mixtures very rich in H_2 are used. Hydrogen molecules in vibrational excited states (H_2^{rv}) can greatly enhance the production of H^- ions in volume and surface by dissociative attachment of hydrogen molecules (DA: $e+H_2(\text{excited}) \rightarrow H + H^-$) [4,5]. To understand the relationship between H_2^{rv} and H^- ions in plasmas, it is vital to investigate the information about the density population over the various energy levels. Many active laser methods have been used for determination of vibrationally excited hydrogen molecules: LIF [6], CARS [7], REMPI [8]. However, these methods are rather complicated and expensive. Furthermore, for many applications it is sufficient to know the relative distribution of vibrational distribution. Optical emission spectrum (OES), due to its simplicity high sensitive resolution and non-intrusive to the discharge system, has the potential of becoming a in-situ diagnostic technique for many application. To determine the rovibrational distribution of H_2 molecules, Fulcher transition, $d\,^3\Pi_u \rightarrow a\,^3\Sigma_g^+$, is more suitable for its relatively strong emission intensity and relatively free from interference by other emission lines. This method involves three states ($X\,^1\Sigma_g^+$, $d\,^3\Pi_u$, $a\,^3\Sigma_g^+$) and two processes (excitation process and radiative process). The determination of rovibrational distribution is dependent on establishing the relationship between the population distribution in the electronic ground and excited state.

The spectroscopic techniques have been used for determination of rovibrational distribution in many systems, such as: helicon-wave plasma [9], expanding thermal arc plasmas [10], beam-plasma system [11], MAP-II plasmas [12] and microwave-powered electron-cyclotron-resonance heating plasmas [13]. In recent years, among various electrical discharge techniques to produce active atoms and radicals, dielectric barrier discharges (DBDs), characterized by the presence of one or two layers of insulator (dielectric barrier) between the two electrodes, have been widely studied due to their relatively simple experimental setup and high operating pressure (from a few to thousands of Torr) [14]. Although the DBD hydrogen plasmas are widely used, there is no report about the rovibrational distribution of H_2 in electronic ground state.

This paper presents a spectroscopic investigation on the effect of rovibrational temperature to the production of H^- ions in dielectric barrier discharge hydrogen plasmas. Based on the diagonal Fulcher band, the rovibrational distribution of H_2 in the ground state has been

[a] e-mail: yongxu@dlut.edu.cn

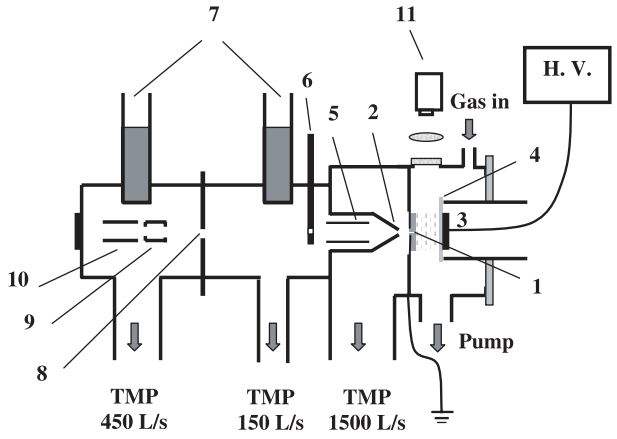

Fig. 1. The schematic diagram of the experimental setup (not to scale). 1: Sampling orifice plate (ground electrode). 2: Skimmer. 3: H.V. electrode. 4: Dielectric (fused silica plate). 5: Ion deflection plate pair. 6: Adjustable valve. 7: Liquid nitrogen trap. 8: Collimation hole. 9: Ionizer. 10: Quadrupole mass analyzer. 11: Monochromator.

determined via optical emission spectrometry. The negative hydrogen ions have also been measured via molecular beam mass spectrometry (MBMS); it is powerful for diagnosis of active species (both ionic and neutral) in moderate pressure [15]. Based on the experimental results, the correlation between the H^- anions density and the vibrational temperature of H_2 molecules has been discussed.

2 Experimental setup

The experimental setup including a DBD reactor, the attached MBMS and OES equipment is schematically illustrated in Figure 1. The vacuum-tight DBD reactor mainly consists of a grounded brass electrode (50 mm in diameter, 5 mm in thickness) and a parallel 5 mm thick fused-silica dielectric barrier plate. The stainless steel high voltage electrode is attached to the outside of the fused-silica plate at atmospheric pressure in order to prohibit the high-voltage breakdown around the fused-silica plate. High purity hydrogen (>99.99%) discharge gas flows through the 10 mm thick gas spacing between the fused-silica dielectric and the ground electrode. The DBD power supply source is capable of supplying a bipolar sine wave output with 0–40 kV peak-to-peak voltage (U_p) at an ac frequency (f_{ac}) of 10–35 kHz.

The grounded brass plate electrode has a central pinhole, which serves as the sampling orifice of the MBMS. In order to reduce the collisions between the detected species and the pinhole walls, the pinhole was made into cone-shape with a thickness of ∼0.1 mm and a diameter of 0.3 mm at the gas-inlet side. The details of the MBMS equipment have been given elsewhere [15,22] and only the main features are outlined here. It consists of a three-stage differential pumping system and a quadrupole mass spectrometer (QMS, EPIC-500N, Hiden Analytical, $m/z = 1-50$ RF source has been used in this work). The region between the sampling plate and the skimmer is called stage 1, which is pumped by a 1500 L/s turbomolecular pump (TMP). The stage 2 with a 150 L/s TMP is located between the skimmer and the collimation hole. The region after the collimation hole where the QMS is located is called stage 3 and it is pumped by a 450 L/s TMP. The stages 2 and 3 were also cooled by liquid nitrogen traps. The pressure in each of the differential pumping stage during sampling with 3 kPa H_2 in the discharge chamber is typically 2×10^{-1}, 1×10^{-3}, and 3×10^{-5} Pa, respectively. The QMS can operate at pressures no higher than 10^{-3} Pa. The low pressure in stage 1 prevents the molecules or ions from undergoing additional collisions after flowing out of the sampling orifice.

The light emitted from plasma was extracted by a quartz lens and then focused on the entrance slit of a 0.5 mm monochromator (Acton, SP-300i, 200–900 nm) via the optical fiber. The optical device response efficiency was calibrated with a standard tungsten lamp (Philips, 10 V, 16–17 A) at known temperature.

3 Spectroscopic method

The technique, called "corona model", used to determine the rovibrational distribution in hydrogen plasmas, is based on the following assumptions: (i) the rotational levels in the electric ground state have a Boltzmann distribution with the same temperature as the Maxwellian distribution of the gas; (ii) the population of the excited $d\,^3\Pi_u$ is mainly by electron impact from the ground state $X\,^1\Sigma_g^+$; (iii) the loss of the excited state $d\,^3\Pi_u$ must be dominated by radiative transition to the other excited $a\,^3\Sigma_g^+$ state. In most plasma sources, these assumptions are taken to be valid in the pressure of the order of tens of microbar [11]. Van der Mullen summarized the criteria for excited levels being in a Corona phase [16]. An effective principal quantum number P is given:

$$P = Z(R_y/|E_{ip}|)^{1/2} \tag{1}$$

here, Z is the charge number of the core, R_y is the Rydberg constant and E_{ip} is the ionization energy from level p. For the level of molecular hydrogen $E_{ip} = 1.6$ eV, $Z = 1$. So the effective principal quantum number $P = 2.9$ can be determined. An approximation for the critical level p_{cr}, below which the Corona phase is valid, is taken from [16]:

$$n_e p_{cr}^9 = 9 \times 10^{23}\ \mathrm{m}^{-3}. \tag{2}$$

The relationship between the electron density n_e and p_{cr} is expressed in Figure 2. The electron density in low-pressure glow discharge plasmas is expected less than 10^{18} m^{-3} [17], so the critical level $p_{cr} \approx 3$ can be determined. Fantz and Heger [13] confirmed the vibrational population of H_2 molecules for the vibrational level $v = 0$–4 can be fairly described by a Boltzmann distribution characterized by a vibrational temperature in divertor plasma, then Xiao et al. [12] also confirmed that the distribution of vibrational (in low levels), and particularly for rotational populations in the ground state of H_2

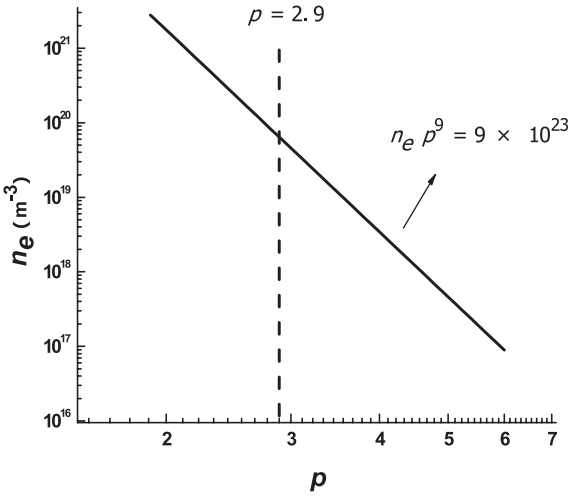

Fig. 2. The critical level p versus the electron density. The dashed line indicates $p = 2.9$.

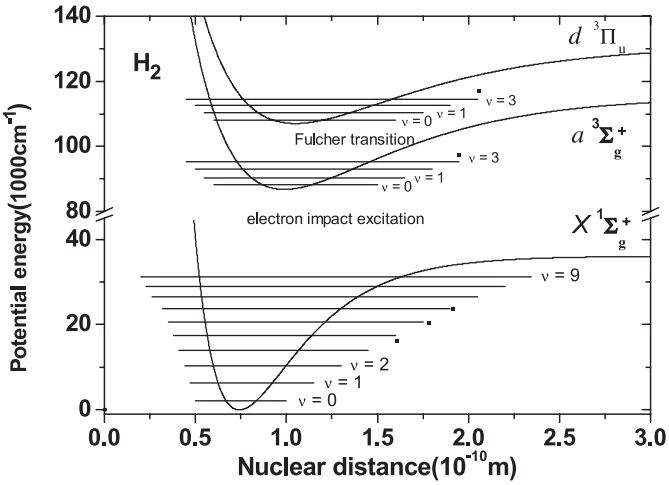

Fig. 3. Potential energy diagram of the levels involved in Corona model.

in low temperature plasmas is fitted to Boltzmann distribution. A more detail discussion can be seen in previous papers [12,13] and therein.

Based on the three assumptions above, the relationship between the optical emission intensity $I^{dv'K'}_{av''K''}$ from the upper $d\,^3\Pi_u$ state to the $a\,^3\Sigma^+_g$ state was expressed by [18]:

$$I^{dv'K'}_{av''K''} = \frac{64\pi^4}{3h\lambda^3}\frac{1}{2K'+1}N_{dv'K'}A^{dv'K'}_{av''K''}. \qquad (3)$$

The intensity is given in photons m^{-3} s^{-1}. Here, h, λ are Plank's constant and wavelength of the emission, respectively. $N_{dv'K'}$ is the density of $d\,^3\Pi_u$ state at vibrational level v' and rotational level K'. The transition probability, $A^{dv'K'}_{av''K''}$, is the product of rotational, vibrational and electronic parts:

$$A^{dv'K'}_{av''K''} = S_{K'K''}q_{v'v''}A_{e'e''} \qquad (4)$$

where $S_{K'K''}$ is called the Honl-London factor and for the Q branch, $S_{KK} = (2K+1)/2$. $q_{v'v''}$ is the Franck-Condo factor.

When a steady state is reached in the discharge plasma, the total production rate for the excited $d\,^3\Pi_u$ state at various vibrational and rotational levels by the electron impact excitation and loss rate by radiative decay to the $a\,^3\Sigma^+_g$ state should be equal. Provided all the assumptions above hold, the following equation can be used to give the rovibrational distribution in ground state:

$$\sum_{v^0}\sum_{K^0}\left\{R^{dv'K'}_{Xv^0K^0}N_{Xv^0K^0}\right\} = N_{dv'K'}A_{tot} \qquad (5)$$

here, R is the electron impact excitation rate from ground state $X\,^1\Sigma^+_g$ to $d\,^3\Pi_u$ state. $N_{Xv^0K^0}$ and $N_{dv'K'}$ are the molecular density at ground state $X\,^1\Sigma^+_g$ and $d\,^3\Pi_u$ state with various vibrational and rotational levels respectively. Figure 3 depicts the potential energy diagram of the levels involved in this balance equation. Indicated are the ground level $X\,^1\Sigma^+_g$, the upper level $d\,^3\Pi_u$ and the lower level of the decay $a\,^3\Sigma^+_g$. The molecular constants of hydrogen in the state in cm^{-1} are taken from [18].

According equations (3) and (5), the relationship between the emission intensity and the rovibrational distribution of the ground state molecules can be given:

$$I^{dv'K'}_{av''K''} = \frac{64\pi^4}{3h\lambda^3}\frac{1}{2K'+1}\frac{A^{dv'K'}_{av''K''}}{A_{tot}}\sum_{v^0}\sum_{K^0}\left\{R^{dv'K'}_{Xv^0K^0}N_{Xv^0K^0}\right\}. \qquad (6)$$

In principle, by the best fit the calculated emission intensity to the experimental results, the rovibrational distribution of the ground state H_2 molecules can be extracted. The Fulcher transition $d\,^3\Pi_u \rightarrow a\,^3\Sigma^+_g$ is the most suitable choice for its relative strong intensity and less disturbance, the emission spectra appear in the wavelength range from 590 to 640 nm. Figure 4 presents the part of the spectra of Fulcher transition for H_2 from dielectric barrier discharge hydrogen plasmas in certain condition ($P(H_2) = 120$ Pa, $U_p = 12$ kV, $f_{ac} = 40$ kHz).

4 Results and discussion

4.1 The determination of vibrational distribution

Based on the validity of Franck-Condo principle for electron impact excitation, the vibrational population in the upper Fulcher $d\,^3\Pi_u$ state could be calculated. The electron impact excitation rate is considered to be proportional to the Franck-Condo factors multiplied by an exponential factor ($e^{-\Delta E_{vib}/kT_e}$) using the energy difference between the vibrational state of interest and $v = 0$ [12,13]. Then, the population density of a vibrational level in the $d\,^3\Pi_u$ state can be related to the ground state by the following equation:

$$f_d(v') \propto \sum_{v^0} q^{dv'}_{Xv^0} f_X(v^0)e^{-\Delta E_{vib}/kT_e} \qquad (7)$$

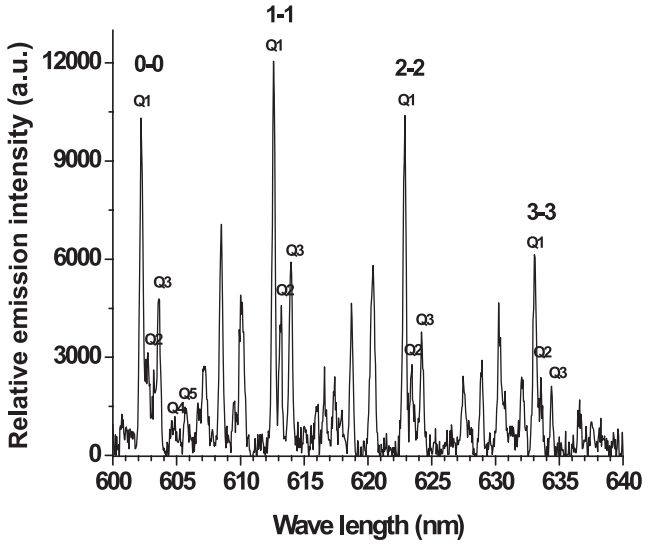

Fig. 4. Typical spectra of the Fulcher band of H_2 measured in low pressure hydrogen DBD plasmas. Discharge conditions: $P(H_2) = 120$ Pa, $U_p = 12$ kV, $f_{ac} = 40$ kHz.

and the intensity for different vibrational band for the Fulcher transition, $d\,^3\Pi_u \rightarrow a^3\Sigma_g^+$, can be expressed by:

$$I_{v''}^{v'} \propto \lambda^{-3} f_d(v') q_{av''}^{dv'}. \tag{8}$$

Here, $f_X(v^0)$ is the vibrational distribution in the ground state. $q_{Xv^0}^{dv'}$ is the Franck-Condo factors from vibrational level v^0 in the $X\,^1\Sigma_g^+$ state to the vibrational level v' in the $d\,^3\Pi_u$ state and $q_{av''}^{dv'}$ is the Franck-Condo factors from vibrational level v' in the $d\,^3\Pi_u$ state to the vibrational level v'' in the $a\,^3\Sigma_g^+$ state. T_e is the average electron energy in plasmas. According to equations (7) and (8), the intensity distribution over the vibrational bands can be calculated from the ground state vibrational temperature, T_{vib}, for any vibrational lines:

$$I_{v''}^{v'} \propto \lambda^{-3} \sum_{v^0} q_{Xv^0}^{dv'} f_X(v^0) e^{-\Delta E_{vib}/kT_e} q_{av''}^{dv'} \tag{9}$$

de Graaf [19] has investigated the influence of the electron temperature on the vibrational intensity distribution. He concluded that for any electron temperature above 2 eV the maximum error made by assuming 3 eV is smaller than 10% for any vibrational intensity $v' = 0$ to 5. For the electron temperature, the typical value in DBD plasmas is about a few eV [20]. Thus, the effect of electron temperature to the intensity distribution is generally neglected under our experimental conditions. For simple, the electron temperature T_e was set to be 6 eV. Figure 5 presents the calculated intensity values, normalized to the (1–1) transition for the rotational level $K = 1$ line in hydrogen as functions of the ground state vibrational temperature. It can be seen the calculated relative intensity of the (0–0) transition are particularly to T_{vib} in the range of a few thousands K, so the (0–0) transition is primarily selection for the determination of T_{vib} [11]. By comparison the measured intensities and calculated value for (0–0) vibrational

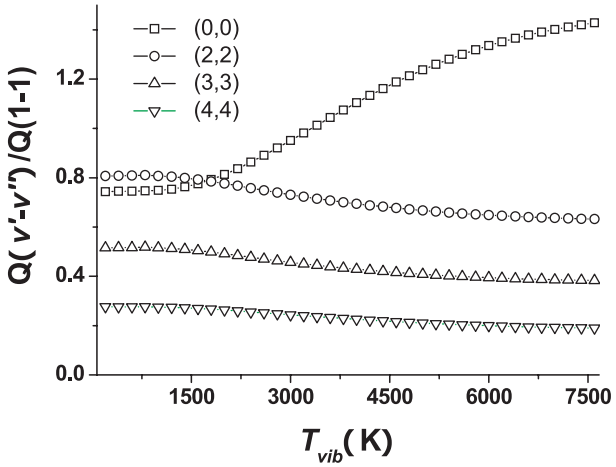

Fig. 5. Evolutions of calculated intensities of the $K' = 1$ in the $v' = v'' = 0$, 2, 3 band normalized to the intensity of $K' = 1$ in the $v' = v'' = 1$ as a function of vibrational temperature.

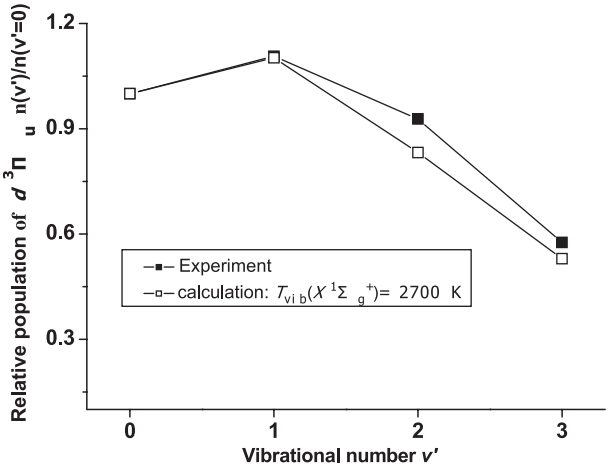

Fig. 6. Comparison of the relative vibrational population of the upper state $d\,^3\Pi_u$ of H_2 by measurement and calculation. Solid square: experiment, hollow square: best-fitted by equation (9).

transition, normalized to the (1–1) transition, a ground state vibrational temperature T_{vib} of about 2700 K can be extracted. The comparisons of vibrational distribution by experiment and the calculation for $v = 1$ to 4 of is shown in Figure 6. The maximum uncertainty of the emission intensity between experimental results and that of calculated is smaller than 10%. It is shown that the calculated relative intensity of (0–0) vibrational transition, normalized to the (1–1) transition is a feasible and simple way to determine the ground state vibrational temperature T_{vib}.

4.2 The determination of rotational distribution

The rotational distributional function is expected to be independent of vibrational state. Similar to vibrational distribution, the population density of a rotational level in the $d\,^3\Pi_u$ state can be related to that of the ground

Table 1. Lines coinciding with lines of the Fulcher-α band within 0.05 nm [26].

"disturbed" line (nm)	"disturbing" lines			
	upper level	lower level	branch	wavelength (nm)
$Q_{0-0}(3)$ 603.1909	$i\,^3\Pi_g(v'=2)$	$c\,^3\Pi_u(v''=2)$	$P(2)$	603.1465
$Q_{1-1}(2)$ 612.7246	$h\,^3\Sigma_g^+(v'=0)$	$c\,^3\Pi_u(v''=0)$	$P(4)$	612.7344
$Q_{1-1}(5)$ 615.9565	$d\,^3\Pi_u(v'=0)$	$a\,^3\Sigma_g^+(v''=0)$	$Q(10)$	615.9269
$Q_{2-2}(1)$ 622.4815	$I\,^1\Pi_u(v'=3)$	$B^1\,\Sigma_g^+(v''=10)$	$Q(3)$	622.5040
	$g\,^3\Sigma_g^+(v'=2)$	$c\,^3\Pi_u(v''=2)$	$P(3)$	622.5312

state by the following equation:

$$f'_{rot}(K') = \sum_{K^0} R_{K^0K'} f^0_{rot}(K^0) = \sum_{K^0} R_{K^0K'} g_{as}(2K^0+1) \exp\left[\frac{-F_{Xv^0}(K^0)hc}{kT_{rot}}\right] \quad (10)$$

here, $R_{K^0K'}$ is the electron impact excitation rate between rotational levels; $f^0_{rot}(K^0)$ is the rotational distribution of ground state [18]; g_{as} is the degeneracy with the nuclear spin. The values of $R_{K^0K'}$ were taken from de Graaf [19]. Then, the rotational line intensity can be calculated by the following equation:

$$I^{K'}_{K''} \propto \lambda^{-3} f'_{rot}(K') = \lambda^{-3} \sum_{K^0} R_{K^0K'} g_{as}(2K^0+1) \times \exp\left[\frac{-F_{Xv^0}(K^0)hc}{kT_{rot}}\right]. \quad (11)$$

By fitting the calculated intensity distribution with that of observed, the rotational temperature could be deduced. The calculation included ground state rotational levels up to $K = 6$ and vibrational levels up to $v = 4$. The section rules of $K = 0, \pm 2, \pm 4$ were included in the calculation processed. In order to determine the rotational temperature correctly, the emission intensity must be strong enough and cannot be disturbed by other emission line. Table 1 presents the possible overlapping lines within 0.05 nm (the resolution of optical system is 0.05 nm). In principle, the rotational temperature can be extracted from emission lines in every vibrational band. However, the vibrational (0–0) band is the most favorable [11,19] as its relative strong emission intensities and more rotational lines could be observed which could reduce the errors. Based on the best-fitted rotational distribution via equation (11) to that of observed experimentally, the rotational temperature of about 400 K was extracted. Figure 7 shows the comparisons of the calculated and observed rotational intensity distribution. The biggest uncertainty of T_{rot} is about 10%. So, it can be concluded that vibrational (0–0) band is very favorable to extract the rotational temperature in our discharge system.

If the time for rotational relaxation is much shorter than that for radiation and other kinetic processes that dead to a redistribution of rotational levels, the rotational temperature may have a certain physical meaning. In this case, the rotational distribution can be described

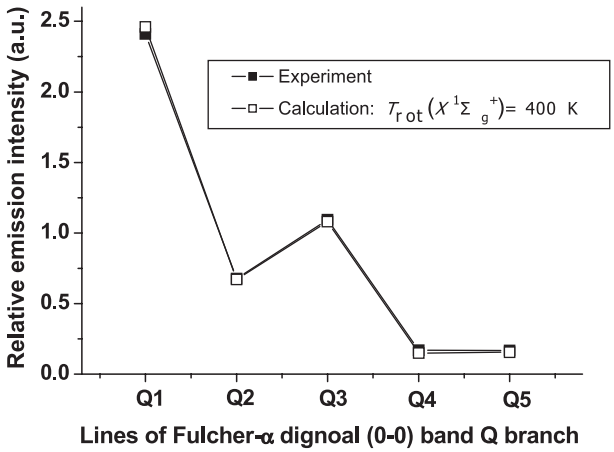

Fig. 7. Comparison of the relative rotational population of the (0–0) band of the Fulcher-α band of H_2 by measurement and calculation. Solid square: experiment, hollow square: best-fitted by equation (11).

by Boltzmann distribution and the rotational temperature is equal to the translational temperature. So, the most convenient way to determine the ground state rotational temperature is to determine an effective rotational temperature T'_{rot} for $d\,^3\Pi_u$ state. The effective temperature is defined as the best straight line fit through the measured in a Boltzmann plot versus the rotational energy. Unfortunately, for the $d\,^3\Pi_u$ state, there is insufficient evidence to support such an assumption. The radiative lifetime of this state is too short to allow it to achieve thermal equilibrium with the working gas [12]. Figure 8 presents the Boltzmann plots of (0–0), (1–1) and (2–2) rotational bands. The effective rotational temperatures at different v' levels are also shown. Some are even below the room temperature. They are 390, 262 and 261 K for (0–0), (1–1) and (2–2) rotational bands, respectively. The results are consistent with that of reported in [12,23]. It can be concluded that the most convenient way to determine the effective rotational temperature is not feasible, at least in one aspect. In contrast, it is more reliable method to determine the rotational temperature in ground state by comparing the experimental results to that of the best mathematic simulation. It is concluded that the Boltzmann distribution for the rotational population in the ground state is a rather good approximation under our experimental conditions. The rotational temperature extracted from (0–0) vibrational band is almost same to that deduced from equation (11), so the vibrational (0–0) band is the most

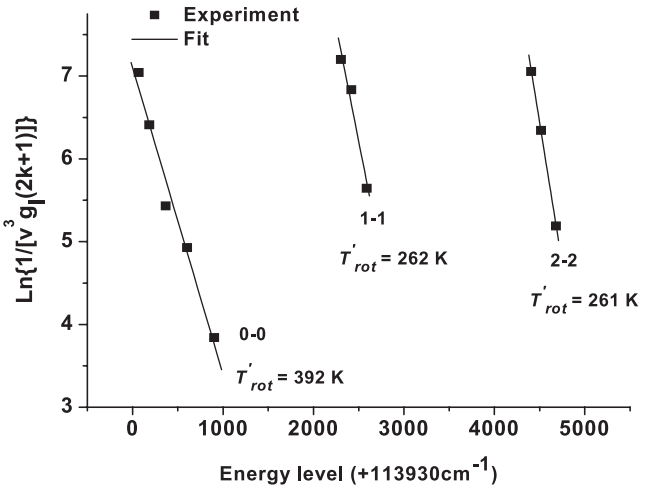

Fig. 8. Boltzmann plot of the Q-branches in the (0–0), (1–1), and (2–2) vibrational bands.

favorable potential to determine the rovibrational distribution of H_2 in ground state [11,19].

4.3 The effect of discharge parameter to the vibrational temperature and density of negative hydrogen ions

The variations of vibrational temperature and mass signal intensity of H^- ions (the absolute deconvoluted mass peak area) are presented in Figures 9b and 9c, respectively. For the plasmas investigated, the vibrational temperatures of the ground state have been found from about 3600 to 2400 K as the pressure increases under the pressure studied. The intensity of H^- ions has the similar tendency. The decrease of vibrational temperature and the intensity of H^- ions with the increase of pressure can be ascribed to the decrease of electron temperature. When the pressure increases, the more energy is transferred from the electrons to the neutrals. It can be also brings about more cooling to the rovibrationally excited H_2 so that the vibrational temperature goes down. It is reasonable to conclude the trend of electron temperature is accordant to that of H atoms excitation temperature calculated from the emission intensity of H_α and H_β line (the calculation method has been discussed in Ref. [21]). From Figure 9a, it can speculate the electron temperature also decreased as the pressure increase. Similar results were also observed in [23], in which hydrogen plasmas were produced in divertor simulator MAP-II. Figure 10 shows the variations of vibrational temperature and mass signal intensity of H^- ions as a function of discharge voltage at a pressure of 120 Pa and discharge frequency of 40 kHz. Both of them rise linearly as discharge increases from 10 to 16 kV. The monotonic increase of vibrational temperature and signal intensity of H^- ions with rising discharge voltage can be mainly ascribed to the increasing electron density and electron temperature as the discharge voltage is increased. This kind of relationship between the electron

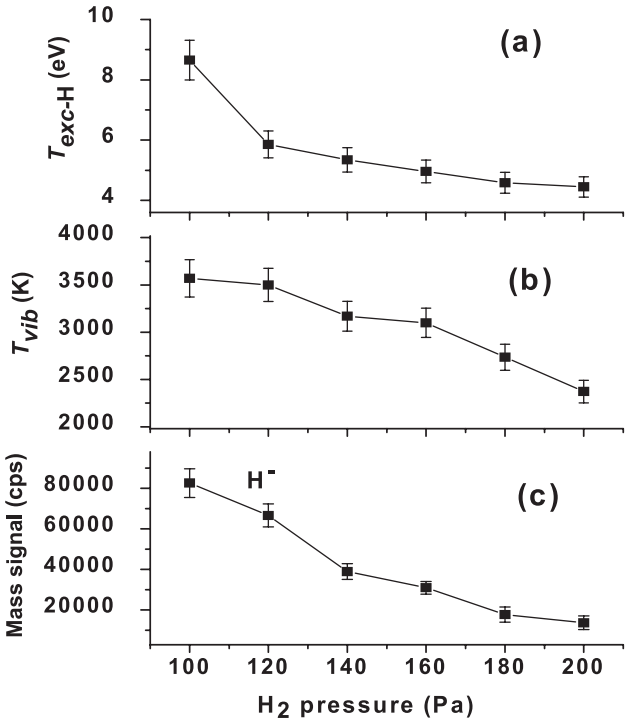

Fig. 9. Measured H atoms excitation temperature (a), vibrational temperature of H_2 (b) and mass signal intensities of H^- anions (c) as functions of H_2 pressure. Discharge conditions: $U_p = 14$ kV, $f_{ac} = 40$ kHz.

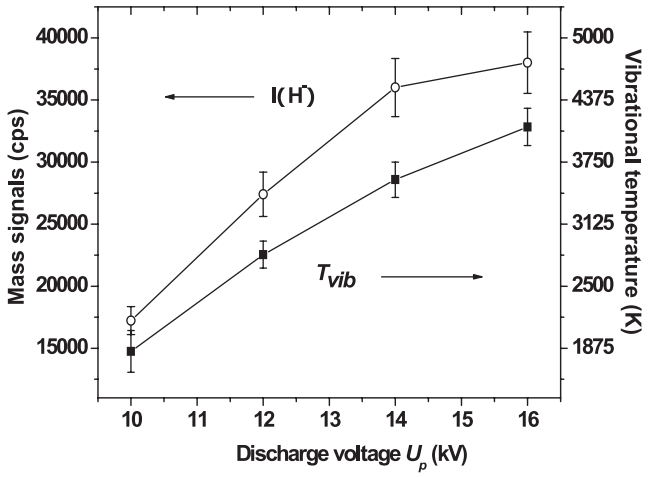

Fig. 10. Evolutions of vibrational temperatures and mass signal intensities of H^- anions as functions of discharge voltage. Discharge conditions: $P(H_2) = 120$ Pa, $f_{ac} = 40$ kHz. Open circles: the mass signals of H^- ions, filled squares: vibrational temperature of H_2 in ground state.

density/temperature and discharge voltage can be found from some experimental measurements [24,25].

The error bars in Figures 9 and 10 show the random errors in the parallel experiments that may be mainly caused by the control accuracies and reproducibility of the discharge gas pressure, discharge voltage and the detection sensitivity of the mass spectrometer. The relative errors in the H^- ions signal intensity caused by selection of different

mass peak line-shape functions in the deconvolution procedures are within ±10%.

5 Conclusions

Rovibrational molecular distribution and negative ions in H_2 dielectric barrier discharge plasmas have been investigated via optical emission spectrometry and molecular beam mass spectrometry, respectively. The vibrational and rotational temperatures have been proposed by fitting the rovibrational intensity distributions observed to those of calculated based on the Corona model. It is shown that the ratio of the $Q_{(0-0)}(1)$ to $Q_{(1-1)}(1)$ line is sensitive for the vibrational temperature in the range of 1500 to 7500 K. At certain discharge conditions (ac 40 kHz, 14 kV of peak-to-peak voltage, 120 Pa), the vibrational temperature and rotational temperature in DBD hydrogen plasmas was extracted to be about 2700 K and 400 K, respectively. With the increase of gas pressure from 100 to 200 Pa, both the vibrational temperature and the negative ions density decrease monotonously. The increase of discharge voltage can lead to the increase of both of hydrogen ions and the vibrational temperature. It can be concluded that the rovibrational temperature in the volume can be qualitatively used for explanation the evolutions of H^- ions produced in plasma.

This work is supported by the National Natural Science Foundation of China under the grant Nos. 10474009 and 10475015.

References

1. K.D. Choquette, R.J. Shul, A.J. Howard, D.J. Rieger, R.S. Freundd, R.C. Weltzel, J. Vac. Sci. Techol. B **13**, 40 (1995)
2. Y. Aoki, S. Aoyama, H. Uetake, K. Morizuka, T. Ohimi, J. Vac. Sci. Techol. A **11**, 307 (1993)
3. S.S. Lee, D.W. Minsek, D.J. Vestyck, P. Chen, Science **263**, 1596 (1994)
4. *Production and Neutralization of Negative Ions and Beans AIP Conference Proceedings*, edited by J.G. Alessi, A. Hershcovitch (AIP, New York, 1994), p. 387
5. C. Gorse, R. Celiberto, M. Cacciator, A. Lagana, M. Capitelli, Chem. Phys. **161**, 211 (1992)
6. T. Mosbach, H.M. Katsch, H.F. Dobele, Phys. Rev. Lett. **85**, 3420 (2000)
7. P. Vankan, D.C. Schram, R. Engeln, Chem. Phys. Lett. **400**, 196 (2004)
8. J.H.M. Bonnie, P.J. Eenshuistra, H.J. Hopman, Phys. Rev. A **37**, 1121(1988)
9. J.K. Wang, W.D. Wu, W.G. Sun et al., High Power Laser Part. Beams **10**, 1513 (2005) (*in Chinese*)
10. D.K. Otorbaev, M.J. De Graaf, M.C.M. Van de Sanden, Contr. Plasma Phys. **35**, 195 (1995)
11. E. Surrey, B. Crowley, Plasma Phys. Control. Fusion **45**, 1209 (2003)
12. B.J. Xiao, S. Kado, S. Kajita, D. Yamasaki, Plasma Phys. Control. Fusion **46**, 653 (2004)
13. U. Fantz, B. Heger, Plasma Phys. Control. Fusion **40**, 2023 (1998)
14. U. Kogelschatz, B. Eliasson, W. Egli, J. Phys. IV Fr. **7**, 47 (1997)
15. W.G. Wang et al., Rap. Commun. Mass Spectrom. **19**, 1159 (2005)
16. J.A.M. Van der Mullen, Phys. Rep. **191**, 109 (1990)
17. Y.B. Golubovskii et al., J. Phys. D: Appl. Phys. **37** 1346 (2004)
18. G. Herzberg, *Molecular Spectra and Molecular Structure, I. Spectra of Diatomic Molecules* (Von Nostrand, Princeton, 1965)
19. M. de Graaf, Ph.D. thesis, Technische Universiteit Eindhoven (1994)
20. X.J. Xu, Thin Solid Films **390**, 237 (2001)
21. Z.C. Geng, Y. Xu, X.F. Yang, W.G. Wang, A.M. Zhu, Plasma Source Sci. Technol. **14**, 76 (2005)
22. D.P. Liu et al., Diamond Relat. Mater. **11**, 1491 (2002)
23. S. Kajita, S. Kado, N. Uchida, T. Shikama, S. Tanaka, J. Nucl. Mater. **313-316**, 748 (2003)
24. W.G. Wang et al., Spectrosc. Spect. Anal. **9**, 1589 (2006) (*in Chinese*)
25. J.H. Kim, Y.H. Choi, Y.S. Hwang, Phys. Plasmas. **13**, 093501 (2006)
26. H.M. Crosswhite, *The hydrogen molecule wavelength table of Gerhard Heinrich Dieke* (Whiley, New York, 1972)